The role of Cysteine 227 in subcellular localization, water permeability, and multimerization of aquaporin-11

Saki Takahashi, Kanako Muta, Hiroko Sonoda, Ayaka Kato, Ahmed Abdeen, Masahiro Ikeda *

Department of Veterinary Pharmacology, University of Miyazaki, Miyazaki 889-2192, Japan

ARTICLE INFO

ABSTRACT

Aquaporin-11 (AQP11) is the latest member of the mammalian water channel protein family to be described. Recent in vivo studies have shown that mutation at Cys[227] causes renal failure. However the importance of Cys[227] for the molecular function of AQP11 is largely unknown. In this study, we examined the subcellular localization, water permeability, and multimerization of AQP11 with a mutation at Cys[227]. Interestingly, cells expressing the mutants had significantly higher osmotic water permeability. In contrast, the mutation lowered the cell surface expression and multimerization levels. Our observations suggest that Cys[227] is crucial for the proper molecular function of AQP11.

1. Introduction

The aquaporins (AQPs) are a family of integral membrane proteins, which transport water and small solutes including glycerol, CO_2, ammonia, urea, and hydrogen peroxide across the membranes of biological cells [1]. So far, sequence analyses have revealed thirteen functionally and phylogenetically distinct members of the AQP family in mammals, of which AQP0, AQP1, AQP2, AQP4, AQP5, AQP6, and AQP8 are orthodox AQPs that primarily transport water molecules, AQP3, AQP7, AQP9, and AQP10 are aquaglyceroporins that are permeated by water and neutral solutes, and AQP11 and AQP12 are a recently proposed third group of AQPs whose functions are largely unknown [1–4].

It has been demonstrated that the orthodox AQPs and aquaglyceroporins share the same molecular architecture [3,5,6]. These proteins exist as multi-subunit oligomers and each subunit has the channel pore. Two highly conserved Asn-Pro-Ala (NPA) motifs in each subunit are present in each member, and these are known to be the signature motifs of the AQPs. Structural analyses have shown that these motifs reside on opposite sides of each monomer and are important for pore formation.

Compared with the orthodox AQPs and aquaglyceroporins, AQP11 and AQP12 are the most distantly related paralogs with low amino acid sequence identity (AQP11 is approximately 10% identical and AQP12 is approximately 25% identical to the sequences of the orthodox AQPs and aquaglyceroporins) [2–4,6–8]. With regard to the signature motifs, the N-terminal NPA motif for AQP11 is Asn-Pro-Cys (NPC) and that for AQP12 is Asn-Pro-Thr (NPT), the C-terminal NPA motif being conserved.

In comparison with AQP12, AQP11 has been better characterized [4,7–10,12]. AQP11 was first described by our group and studies with AQP11-deficient ($Aqp11^{-/-}$) mice revealed the importance of AQP11 during post-natal kidney development in mammals [7]. Immunohistochemical studies showed that AQP11 was localized mainly in the endoplasmic reticulum (ER) in certain tissues such as kidney, liver, testis, intestine, and brain. An osmotic water permeability assay with Sf9 membrane vesicles and mammalian cells expressing AQP11 indicated that AQP11 was a water-permeable channel [8,9].

Recently, Tchekneva and colleagues have characterized sudden juvenile death syndrome (sjds) mutation ($Aqp11^{sjds/sjds}$) mice that are characterized by cell injury in the renal cortex, resembling the phenotype of $Aqp11^{-/-}$ [10]. They also identified the Cys[227] to Ser mutation in $Aqp11^{sjds/sjds}$ mice as the causative mutation and found that the phenotype of heterozygous $Aqp11^{-/sjds}$ compound mice was similar to that of $Aqp11^{-/-}$ mice, indicating that the Cys[227] to Ser mutation was a loss-of-function one. However, the importance of Cys[227] for the molecular function of AQP11 has yet to be elucidated.

In order to gain insight into the nature of AQP11, we examined the role of Cys[227] in AQP11 in terms of subcellular localization, water permeability, and multimerization in transfected mammalian cells.

Unexpectedly, the mutation at Cys^{227} was found to confer a gain-of-function in terms of water permeability, suggesting that Cys^{227} is crucial for the proper molecular function of AQP11.

2. Materials and methods

2.1. Plasmid construction, cell culture, transfection and confocal microscopy

Constructs encoding Myc-, green fluorescent protein- (GFP-), or DsRed-Monomer- (DsRM-) -tagged proteins were made by in-frame subcloning of human AQP11 into pCMV-Myc (BD Biosciences Clontech, CA), pEGFP-C1 (BD Biosciences Clontech), or pDsRed-Monomer (BD Biosciences Clontech). C-terminal GFP-tagged human AQP1 (AQP1-GFP) was also made by in-frame subcloning of human AQP1 into pcDNA-DEST47 (Invitrogen, CA). For fluorescence labeling of the ER, the pDsRed2-ER vector (BD Biosciences Clontech) was employed. A site directed mutagenesis kit (Stratagene, CA) was used to introduce the mutations of the constructs.

CHO-K1 cells (obtained from ATCC, #CCL-61) were transfected at 50–60% confluency using Lipofectamine 2000, Lipofectamine LTX (Invitrogen), or a Neon® Transfection System in accordance with the manufacturer's instructions. A Neon® Transfection System was employed only to examine the total expression level of DsRM-hAQP11-C227S. When fluorescence microscopy was conducted, cells on glass coverslips were observed 24 h after transfection using a laser scanning confocal microscope (Olympus FV300, Tokyo, Japan).

2.2. Surface biotinylation

A cell surface biotinylation assay was performed as described previously [8]. Briefly, transfected cells were biotinylated in 1 mg/ml sulfo-NHS-SS-biotin (Pierce, IL) at 4 °C for 10–15 min, washed, and then lysed in lysis buffer (25 mM Tris, pH 7.4, 150 mM NaCl, 2 mM EDTA, 2% Nonidet P-40, Complete protease inhibitor mixture) for 20 min at 4 °C. The cell lysate was centrifuged at 12,000g for 10 min, and the supernatant was precipitated with immobilized NeutrAvidin beads (Pierce).

2.3. Cross-linking experiments

Cross-linking with paraformaldehyde was performed as described previously [8]. Briefly, cells were incubated with PBS containing 4% paraformaldehyde at room temperature for 15 min. After washing, the cells were lysed in lysis buffer (25 mM Tris, pH 7.4, 150 mM NaCl, 2 mM EDTA, 1.5% Nonidet P-40, Complete protease inhibitor mixture) and the lysate was then mixed with 2× Laemmli sample buffer supplemented with 0.1 M DTT at 37 °C for 20 min.

2.4. Measurement of osmotic water permeability (Pf)

One day after transfection, cells were treated with trypsin–EDTA for a short time (around 15 s) to create a round cell shape, allowing easy calculation of cell volume [8]. The rounded cells were then washed and bathed in an extracellular solution (ES) containing (in mM) 150 NaCl, 1 MgCl₂, 1 CaCl₂, and 10 Hepes (pH 7.4 with Tris). The cells expressing DsRM were identified under a laser scanning confocal microscope. Osmotic swelling was caused by puff-application of a hypotonic solution made by 1:1 dilution of ES in MilliQ water at room temperature (around 25 °C), as described previously [8,11]. An image frame of each cell was recorded every 1.12 s using a time-lapse image-capture system attached to the laser scanning confocal microscope. Pf was calculated from osmotic swelling data using the formula:

$$Pf = [V_0 \times d(V/V_0)/dt]/[S \times V_w \times (\text{osm}_{\text{in}} - \text{osm}_{\text{out}})]$$

where V_0 and S are the initial cell volume and surface area, respectively, $d(V/V_0)/dt$ is the slope of linear fit for the plot of cell volume vs. time between 1.12 and 17.92 s during osmotic swelling, and $V_w \times (\text{osm}_{\text{in}} - \text{osm}_{\text{out}})$ is the osmolality gradient.

2.5. Western blot analysis and chemicals

After separation by SDS–PAGE, the protein was transferred to a polyvinylidene difluoride membrane and the protein on the membrane associated with antibodies was detected by a Super Signal® chemiluminescence detection system (Pierce). The anti-Myc antibody was from BD Biosciences Clontech. All other chemicals and reagents were from Sigma or Wako Pure Chemicals (Japan).

3. Results

3.1. Subcellular localization of the AQP11 mutants at Cys^{227}

AQP11 has been shown to be localized at the ER membrane [7,8]. We investigated whether the introduction of a mutation at Cys^{227} replacing it with Ser (C227S) or Ala (C227A) affected the subcellular localization of AQP11. In this experiment, we used C-terminal GFP-tagged human AQP1 (hAQP1-GFP) as a control protein and N-terminal GFP-tagged human AQP11 (GFP-hAQP11), because it has been reported that the N-terminus of AQP1 functions as a signal for the proper localization, and tagging of GFP to the N- and C-terminus of AQP11 resulted in virtually the same subcellular localization [8,12]. When CHO cells were transfected with hAQP1-GFP expression plasmid together with a plasmid encoding an ER marker protein, hAQP1-GFP was clearly localized at the plasma membrane as well as at the ER (Fig. 1A–C), in line with a previous observation [8]. In contrast, the localization of GFP-hAQP11 virtually overlapped that of the ER marker (Fig. 1D–F). Similarly to GFP-hAQP11, GFP-hAQP11-C227S, and -C227A were clearly localized at the ER.

It has been shown that although the level of AQP11 expression is less than that at the ER, a significant amount of the protein is expressed at the plasma membrane [8]. Therefore, we checked the cell surface expression levels of Myc-hAQP11, Myc-hAQP11-C227S, and Myc-hAQP11-C227A using a cell surface biotinylation assay. The levels of both total and biotinylated protein for Myc-hAQP11-C227S and Myc-hAQP11-C227A were significantly lower than those of the wild type (Fig. 2A and B). On the other hand, the ratio of the level of biotinylated protein to that of total protein was not significantly altered between the wild type, Myc-hAQP11-C227S, and Myc-hAQP11-C227A (Fig. 2C).

It is possible that when using a chemically based lipofection technique to introduce a plasmid into cells, transfection efficiency may differ according to the plasmid employed, which might result in a reduced level of mutant expression being observed. Therefore, we also compared the total expression level of DsRM-hAQP11-C227S with that of DsRM-hAQP11 using electroporation, a mechanical transfection technique that is considered to introduce a fairly constant amount of plasmid into cells, even if different plasmids are used. The results showed that the protein expression level of DsRM-hAQP11-C227S was reduced by about 25% ($n = 3$) relative to that of its wild-type, thus corroborating the results obtained using Myc-tagged proteins.

Taken together, these data indicated that introduction of the mutation at Cys^{227} of AQP11 decreased the total level of expression, but did not affect trafficking to the plasma membrane.
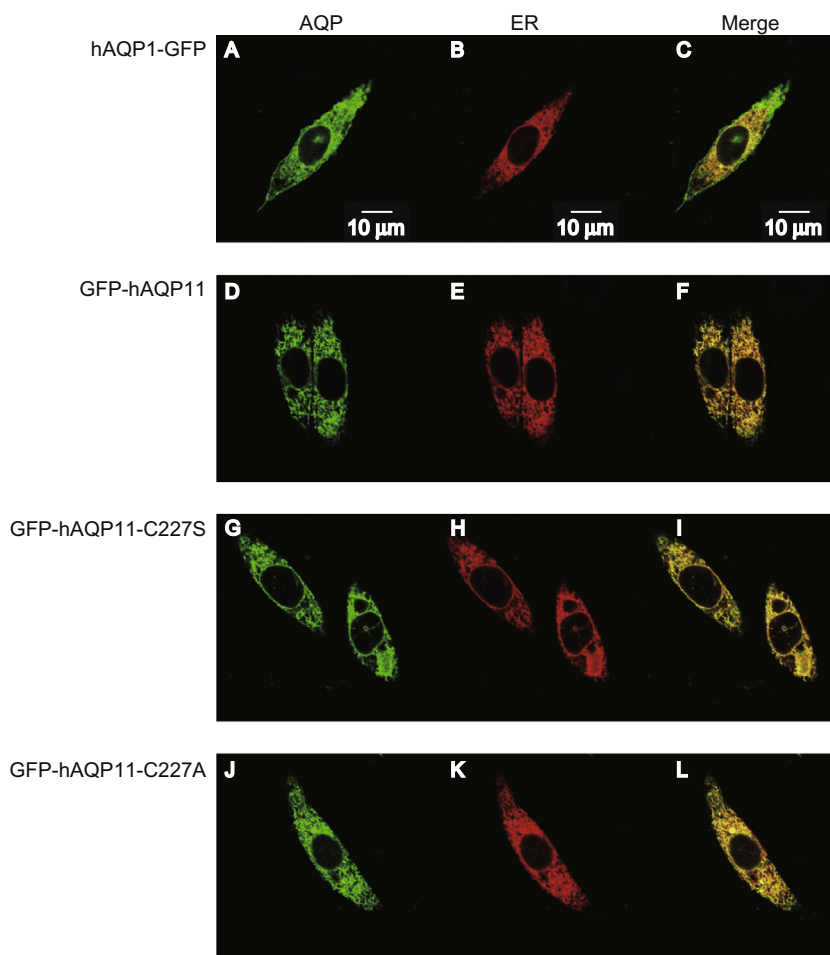
Fig. 1. Subcellular localization of AQP11 mutants at Cys^{227}. (A–L) Subcellular localizations of hAQP1-GFP (A–C), GFP-hAQP11 (D–F), GFP-hAQP11-C227S (G–I), and GFP-hAQP11-C227A (J–L) were evaluated by fluorescence microscopy. CHO cells were co-transfected with each AQP expression plasmid and a plasmid encoding an ER marker protein. Green (A, D, G, and J) and red (B, E, H, and K) colors indicate AQPs and ER marker proteins, respectively. The merged images are also shown (C, F, I, and L). The images were obtained 24 h after transfection. Scale bars = 10 μm. (For interpretation of the references to colour in this figure legend, the reader is referred to the web version of this article.)

3.2. Osmotic water permeability (Pf) of the AQP11 mutants at Cys^{227}

Cell surface biotinylation experiments showed that significant amounts of AQP11 and its mutants were also expressed at the plasma membrane (Fig. 2), and we had previously reported that the level of AQP11 cell surface expression allowed us to measure water permeability by an osmotic swelling assay [8]. Therefore, we employed this assay system and examined the osmotic water permeability of cells expressing DsRM-hAQP11, DsRM-hAQP11-C227S, or DsRM-hAQP11-C227A. As shown in Fig. 3A, hypotonic stimulation unexpectedly caused more rapid swelling of cells expressing DsRM-hAQP11-C227S and DsRM-hAQP11-C227A than that of cells expressing the wild type. The Pf values (Fig. 3B) of DsRM-hAQP11-C227S and -C227A were significantly higher than that of wild-type AQP11. It was noted that the Pf value shown as mean ± SE was 4.7 ± 0.9 cm/s $\times 10^{-4}$ ($n = 6$) for the mock cells. As the plasma membrane expression levels of mutants were significantly lower than that of the wild type (Fig. 2), these data suggest that the mutation of AQP11 at Cys^{227} conferred a gain of function for water permeability.

3.3. Multimeric structure of the AQP11-C227A mutant

We have shown that AQP11 is able to form a multimerized structure [8]. Recently, our group also observed the reduced multimer formation of AQP11-C227S using a cross-linker, paraformaldehyde [13]. We therefore evaluated the multimeric structure of AQP11-C227A using the same method. As shown in Fig. 4A, paraformaldehyde was able to clearly produce a band at ∼75 and ∼50 kDa in addition to a band at ∼25 kDa for Myc-hAQP11, confirming that AQP11 has a multimerized structure. In contrast, when Myc-hAQP11-C227A was examined, the bands at ∼75 and ∼50 kDa were missing, but the band at ∼25 kDa was visible. Even when we employed a 20-fold longer exposure time, no bands at ∼75 kDa were evident (Fig. 4B). Fig. 4C shows the summarized data for Fig. 4A, indicating a reduced ability of Myc-hAQP11-C227A to form a multimerized protein in comparison with the wild-type protein. Taken together with the reported data, these results indicate that Cys^{227} of AQP11 has an important role in homo-multimerization.

4. Discussion

Aqp11$^{sjds/sjds}$ mice generated using a powerful chemical mutagen, n-ethyl-n-nitrosourea (ENU), have been characterized [10]. The mice died before 3 weeks of age, whereas heterozygous sjds and wild-type siblings were phenotypically normal. The cause of the death of the Aqp11$^{sjds/sjds}$ mice was kidney failure, accompanied by proximal cell injury in the cortex. The pathological changes evident in this type of proximal cell injury included cytoplasm
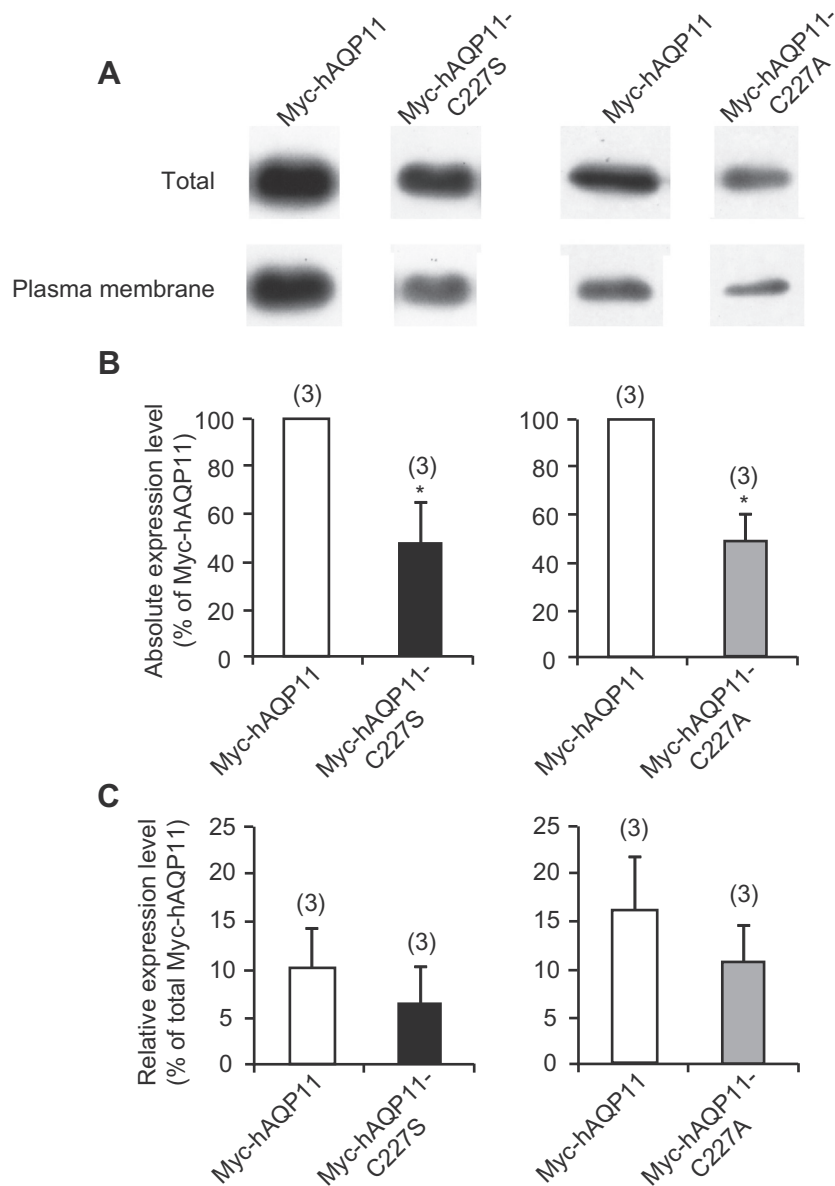
Fig. 2. Cell surface expression level of AQP11 mutants at Cys^{227}. (A) Cell surface expression levels of Myc-AQP11, Myc-hAQP11-C227S, and Myc-hAQP11-C227A were assessed by a biotinylation experiment. CHO cells were transfected with Myc-AQP11 or its mutant protein expression plasmid, and 24 h after transfection the cell surface proteins were labeled with membrane-impermeable biotin. The biotin-labeled proteins were precipitated by NeutrAvidin beads. The biotin-labeled cell surface proteins, as well as the total cell lysates, were analyzed by Western blotting using anti-Myc antibody. The Western blot image is separately shown, because the original image included data for the other sample in the middle lane between the Myc-hAQP11 and Myc-hAQP11-C227S, or Myc-hAQP11-C227A samples. The separate image originated from the same blot, while retaining the original quality. (B) The absolute cell surface expression level is summarized. Each value is expressed as a percentage of the mean value for Myc-hAQP11. Data are shown as means ± SE. The numbers of experiments are given in parentheses. $^*P < 0.05$ compared with the Myc-hAQP11 group (Mann–Whitney U test). (C) The ratio of biotinylated to total Myc-tagged proteins was taken as an index of the relative surface expression level. Values are presented as mean ± SE. No significant difference was found between Myc-hAQP11 and Myc-hAQP11-C227S, or Myc-hAQP11-C227A (Student's t test).

vacuolization, nuclear swelling, and mitochondrial injury. As these phenotypes closely resembled those of AQP11$^{-/-}$ mice [7,10], the Aqp11 gene of Aqp11$^{sjds/sjds}$ mice was sequenced and a T-to-A transversion was found at codon 718 in exon 2, resulting in substitution of Cys^{227} by Ser. Finally, Aqp11$^{-/sjds}$ heterozygous compound mice were generated, and their phenotype was very similar to those of Aqp11$^{sjds/sjds}$ and Aqp11$^{-/-}$ mice, suggesting that the Cys^{227} to Ser mutation in Aqp11 was an inactivating mutation, and responsible for the phenotype of Aqp11$^{sjdsj/sjds}$ mice. In the present study, a cell surface biotinylation assay clearly indicated that the mutation at Cys^{227} decreased the expression level of AQP11 at the plasma membrane as well as the total expression level. In contrast, the cells expressing AQP11-C227S or -C227A

unexpectedly had significantly higher osmotic water permeability than that of wild-type AQP11 (Fig. 3). These in vitro data indicate that the mutation at Cys^{227} resulted in an increase of AQP11 water transport activity. How can these in vivo loss-of-function and in vitro gain-of-function data be reconciled? One possible answer is that the number of correctly localized functional AQP11 molecules is dramatically reduced in the kidney of Aqp11$^{sjdsj/sjds}$ mice, compared with that of AQP11-C227S in transfected cells. In fact, it has been reported that the level of AQP11-C227S mRNA in samples of AQP11$^{sjds/sjds}$ mutant kidney was dramatically reduced [10]. Also, although we were unable to observe the unusual oligomerized protein form of AQP11-C227S in vitro (data not shown), this form was found to be increased in the Aqp11$^{sjds/sjds}$ renal cortex
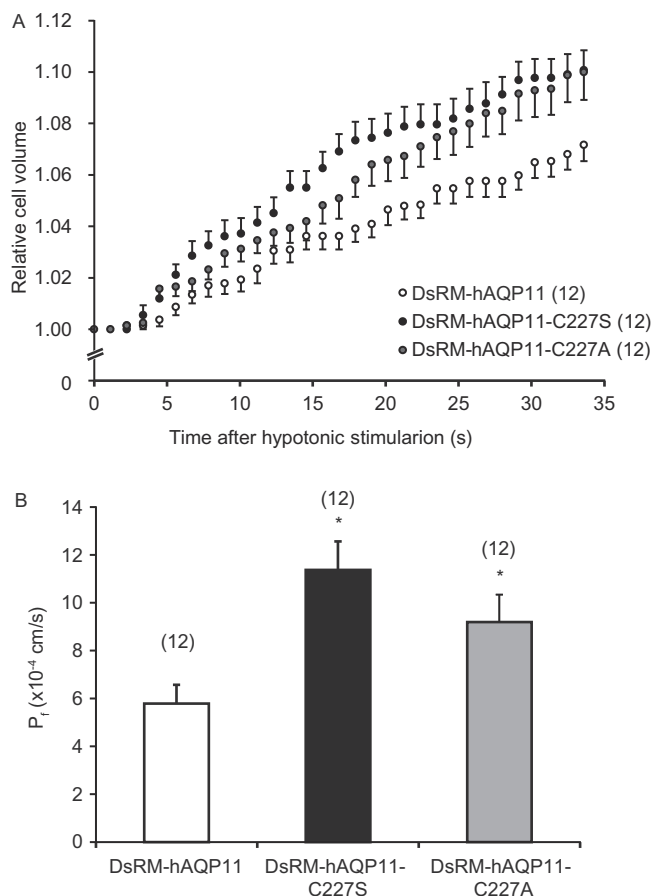
Fig. 3. Osmotic water permeability of cells expressing AQP11 mutant at Cys227. (A) CHO cells were transfected with DsRM-AQP11, DsRM-hAQP11-C227S, or DsRM-hAQP11-C227A expression plasmid. After 24 h, the cell diameter was measured under a microscope. The cells were exposed to hypotonic solution (300–150 m Osm/kg solution) at time point of 0. An image of the cell was recorded every 1.12 s with the microscope equipped with a time-lapse image-capture system. Values are presented as mean ± SE. The numbers of cells tested are given in parentheses. (B) Pf values were calculated from osmotic swelling data from A using the formula as indicated in the Materials and Methods. Values are shown as mean ± SE. *P < 0.05 vs. DsRM-hAQP11 (Dunnett's test).
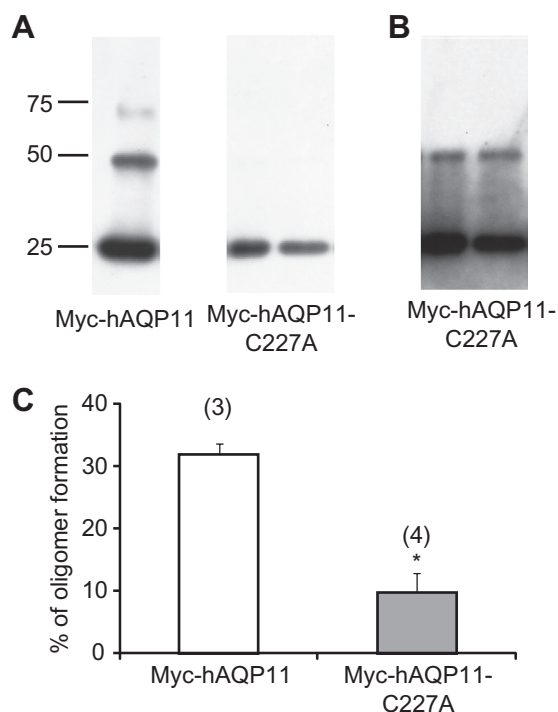

Fig. 4. Oligomerization of the AQP11-C227A mutant. (A) Oligomerization state of Myc-hAQP11 or Myc-hAQP11-C227A was evaluated using a chemical cross-linker, paraformaldehyde. Typical examples of multimerization of Myc-hAQP11 (far left lane) and Myc-hAQP11-C227A (2nd and 3rd lanes from the left) are shown. (B) Corresponding data in 2nd and 3rd lanes from the left of A at 20-fold longer exposure time. (C) The results of densitometric analysis of cross-linked Myc-hAQP11 (white bar) and Myc-hAQP11-C227A (grey bar) are shown. The ratio of multimerized proteins (more than dimer) to total proteins (monomer + multimerized proteins) was taken as an index of the multimerization level. Values are presented as mean ± SE. The numbers of experiments are given in parentheses. *P < 0.05 vs. Myc-hAQP11 (Student's t-test).

by native gel electrophoresis analysis [13]. These data suggest that the reduction of transcription and increase in the formation of an unusual protein structure appear to be involved in the decrease in the number of proper functional protein molecules in the kidney of Aqp11[sjdsj/sjds] mice.

Another possible explanation is that AQP11 is a multi-functional protein, and that a function other than water transport activity, which requires Cys[227], is important for the renal phenotype in AQP11-deficient mice. In fact, it has been reported that the water permeability of AQP11 is 8-fold lower than that of AQP1 (an orthodox AQP) [9]. Furthermore, our group previously showed that primary-cultured proximal tubules from Aqp11^{−/−} mice had impaired endosomal acidification without any change in endosomal Cl^{−} concentration [7]. Together, these data suggest that AQP11 regulates the proton pump and/or sodium-hydrogen exchanger without involvement of its water transport activity, indicating that AQP11 has another role.

A precise explanation for the difference between the in vivo loss-of-function and in vitro gain-of-function results awaits further investigations, including quantification of the amount of functional AQP11 in vivo and exact determination of the molecular function of AQP11.

Many structural studies have demonstrated that orthodox AQPs share the same structural architecture [3,5,6]. The AQPs form oligomers with each monomer functioning as an independent pore and the monomer is built from six transmembrane domains (H1 helix–H6 helix) connected to each other by five loops (loop A–loop E) with two conserved NPA motifs in loops B and E. These two NPA motifs constrict the pore in the middle of the permeation channel. Another narrow constriction, known as the aromatic/Arg (ar/R) filter, is located on the periplasmic side of the channel. This filter is formed by a strictly conserved Arg and an aromatic residue including Phe in the orthodox AQPs. As mentioned earlier, the water permeability of AQP11 is rather low, and similar to that of AQP0. Based on this observation, Yakata et al. have built a model for mouse AQP11 starting with the AQP0 structure (PDB: 2B6O; Gonen et al. [9,14]. As previous studies of the crystallographic structure and molecular dynamics [15,16] had suggested that the Tyr[23] of AQP0 in the H1 helix might contribute to its slow water permeation, the authors described the importance of Tyr[83] in AQP11, located at a similar height along the pore axis as that for AQP0, for slow water permeation in the former. Furthermore, Calvanese et al. [6] have recently reported a 3D-model for AQP11 using a multi-template comparative modeling technique and shown that Tyr[83] of AQP11 is involved in narrowing of the pore in the central region along the pore axis. Therefore, using commercially available software, we constructed rough 3D structural models of both AQP11 and AQP11-C227S using the AQP0 crystal structure as a template. The model indicated that the mutation at Cys[227] did not cause a misalignment of Tyr[83] (data not shown). Therefore, Tyr[83] might not be contributed to the increased water permeability of AQP11-C227S. Future crystallographic studies will be helpful for

clarifying how the mutation increases the water permeability of AQP11.

Our present cross-linking experiment demonstrated that Myc-AQP11-C227A had a lower ability to form multimeric structure. Also, using the same cross-linker, we found that Myc-AQP11-C227S was a less multimerized protein than wild-type AQP11 [13]. These data strongly suggest that Cys[227] of AQP11 plays an important role in formation of its quaternary structure. So far, residues in the N-terminal domain, H1 helix, loop A, H2 helix, H4 helix, H5 helix, and/or C-terminal domain have been suggested to be involved in the formation of tetramer in the AQPs [3,5,17–20]. Also, recently the loop A was reported to be a controller of hetero-oligomerization in the plant AQPs [21]. According to the three-dimensional models built by Yakata et al. and Calvanese et al., Cys[227] of AQP11 is located on the periplasmic side of the membrane (loop E), being exposed on the surface of the protein [6,9]. Also, our rough 3D structural models indicated that the mutation of Cys[227] caused a misalignment of the loop E on the periplasmic side of the membrane. The periplasmic structure of loop E does not appear to be directly involved in formation of the quaternary structure of AQP11. Again, future crystallographic studies will also be necessary to clarify more definitively the quaternary structure of AQP11.

Obviously molecular and biological functions of AQP11 remain to be elucidated and experiments with animals, cells, proteins, and genes are expected to provide conclusive answers to many questions, which are still open. However, we believe that our results broaden previous findings on the significant role of Cys[227] in the expression of molecular function of AQP11.

Author contributions

S.T., K.M., and M.I. designed research; S.T., K.M., H.S., A.K., A.A., and M.I. performed research; S.T., K.M., and M.I. analyzed data; and S.T., H.S., and M.I. wrote the paper.

Acknowledgements

References

[1] Carbrey, J.M. and Agre, P. (2009) Discovery of the aquaporins and development of the field. Handb. Exp. Pharmacol. 190, 3–28.
[2] Zardoya, R. (2005) Phylogeny and evolution of the major intrinsic protein family. Biol. Cell 97, 397–414.
[3] Walz, T., Fujiyoshi, Y. and Engel, A. (2009) The AQP structure and functional implications. Handb. Exp. Pharmacol. 190, 31–56.
[4] Ishibashi, K., Tanaka, Y. and Morishita, Y. (2013) The role of mammalian superaquaporins inside the cell. Biochim. Biophys. Acta, http://dx.doi.org/10.1016/j.bbagen.2013.10.039.
[5] Murata, K., Mitsuoka, K., Hirai, T., Walz, T., Agre, P., Heymann, J.B., Engel, A. and Fujiyoshi, Y. (2000) Structural determinants of water permeation through aquaporin-1. Nature 407, 599–605.
[6] Calvanese, L., Pellegrini-Calace, M. and Oliva, R. (2013) In silico study of human aquaporin AQP11 and AQP12 channels. Protein Sci. 22, 455–466.
[7] Morishita, Y., Matsuzaki, T., Hara-chikuma, M., Andoo, A., Shimono, M., Matsuki, A., Kobayashi, K., Ikeda, M., Yamamoto, T., Verkman, A., Kusano, E., Ookawara, S., Takata, K., Sasaki, S. and Ishibashi, K. (2005) Disruption of aquaporin-11 produces polycystic kidneys following vacuolization of the proximal tubule. Mol. Cell. Biol. 25, 7770–7779.
[8] Ikeda, M., Andoo, A., Shimono, M., Takamatsu, N., Taki, A., Muta, K., Matsushita, W., Uechi, T., Matsuzaki, T., Kenmochi, N., Takata, K., Sasaki, S., Ito, K. and Ishibashi, K. (2011) The NPC motif of aquaporin-11, unlike the NPA motif of known aquaporins, is essential for full expression of molecular function. J. Biol. Chem. 286, 3342–3350.
[9] Yakata, K., Tani, K. and Fujiyoshi, Y. (2011) Water permeability and characterization of aquaporin-11. J. Struct. Biol. 174, 315–320.
[10] Tchekneva, E.E., Khuchua, Z., Davis, L.S., Kadkina, V., Dunn, S.R., Bachman, S., Ishibashi, K., Rinchik, E.M., Harris, R.C., Dikov, M.M. and Breyer, M.D. (2008) Single amino acid substitution in aquaporin 11 causes renal failure. J. Am. Soc. Nephrol. 19, 1955–1964.
[11] Ikeda, M., Beitz, E., Kozono, D., Guggino, W.B., Agre, P. and Yasui, M. (2002) Characterization of aquaporin-6 as a nitrate channel in mammalian cells. Requirement of pore-lining residue threonine 63. J. Biol. Chem. 277, 39873–39879.
[12] Beitz, E., Liu, K., Ikeda, M., Guggino, W.B., Agre, P. and Yasui, M. (2006) Determinants of AQP6 trafficking to intracellular sites versus the plasma membrane in transfected mammalian cells. Biol. Cell 98, 101–109.
[13] Atochina-Vasserman, E.N., Biktasova, A., Abramova, E., Cheng, D.S., Polosukhin, V.V., Tanjore, H., Takahashi, S., Sonoda, H., Foye, L., Venkov, C., Ryzhov, S.V., Novitskiy, S., Shlonimskaya, N., Ikeda, M., Blackwell, T.S., Lawson, W.E., Gow, A.J., Harris, R.C., Dikov, M.M. and Tchekneva, E.E. (2013) Aquaporin 11 insufficiency modulates kidney susceptibility to oxidative stress. Am. J. Physiol. Renal Physiol. 304, F1295–F1307.
[14] Gonen, T., Cheng, Y., Sliz, P., Hiroaki, Y., Fujiyoshi, Y., Harrison, S.C. and Walz, T. (2005) Lipid-protein interactions in double-layered two-dimensional AQP0 crystals. Nature 438, 633–638.
[15] Jensen, M.Ø., Dror, R.O., Xu, H., Borhani, D.W., Arkin, I.T., Eastwood, M.P. and Shaw, D.E. (2008) Dynamic control of slow water transport by aquaporin 0: implications for hydration and junction stability in the eye lens. Proc. Natl. Acad. Sci. USA 105, 14430–14435.
[16] Qiu, H., Ma, S., Shen, R. and Guo, W. (2010) Dynamic and energetic mechanisms for the distinct permeation rate in AQP1 and AQP0. Biochim. Biophys. Acta 1798, 318–326.
[17] Mathai, J.C. and Agre, P. (1999) Hourglass pore-forming domains restrict aquaporin-1 tetramer assembly. Biochemistry 38, 923–928.
[18] Jung, J.S., Preston, G.M., Smith, B.L., Guggino, W.B. and Agre, P. (1994) Molecular structure of the water channel through aquaporin CHIP. The hourglass model. J. Biol. Chem. 269, 14648–14654.
[19] Duchesne, L., Pellerin, I., Delamarche, C., Deschamps, S., Lagree, V., Froger, A., Bonnec, G., Thomas, D. and Hubert, J.F. (2002) Role of C-terminal domain and transmembrane helices 5 and 6 in function and quaternary structure of major intrinsic proteins: analysis of aquaporin/glycerol facilitator chimeric proteins. J. Biol. Chem. 277, 20598–20604.
[20] Cui, Y. and Bastien, D.A. (2012) Molecular dynamics simulation and bioinformatics study on yeast aquaporin Aqy1 from Pichia pastoris. Int. J. Biol. Sci. 8, 1026–1035.
[21] Jozefkowicz, C., Rosi, P., Sigaut, L., Soto, G., Pietrasanta, L.I., Amodeo, G. and Alleva, K. (2013) Loop A is critical for the functional interaction of two Beta vulgaris PIP aquaporins. PLoS One 8, e57993.